11th World Congress on Computational Mechanics (WCCM XI)
5th European Conference on Computational Mechanics (ECCM V)
6th European Conference on Computational Fluid Dynamics (ECFD VI)
E. Oñate, J. Oliver and A. Huerta (Eds)

MODELING OF REYNOLDS-STRESS AUGMENTATION IN SHEAR LAYERS WITH STRONGLY CURVED VELOCITY PROFILES

RENÉ-DANIEL CÉCORA*, ROLF RADESPIEL* AND SUAD JAKIRLIĆ†

* Institute of Fluid Mechanics
Technische Universität Braunschweig
Hermann-Blenk-Str. 37, 38108 Braunschweig, Germany
e-mail: r-d.cecora@tu-bs.de, web page: www.tu-braunschweig.de/ism

† Institute of Fluid Mechanics and Aerodynamics
Technische Universität Darmstadt
Alarich-Weiss-Str. 10, 64287 Darmstadt, Germany
web page: http://www.sla.tu-darmstadt.de/sla

Key words: RANS, Reynolds-stress turbulence modeling, free shear flows

Abstract. An extension and re-calibration of a differential Reynolds-stress model is performed, which is influential in shear layers where the velocity profile shows large second derivatives. Besides a backward-facing step flow and a zero-pressure-gradient flat plate, which are used for calibration, further test cases are simulated with the new model for validation purposes. Especially the simulation of the flow over a transonic bump can be improved with the new model version JHh-v3, further improvements are made for a turbulent round jet.

1 INTRODUCTION

Numerical flow simulation is an important tool in the development process of aircraft industry. Solving of the *Reynolds-Averaged Navier-Stokes* (RANS) equations is regarded as a good compromise between computational effort and accuracy. The quality of RANS simulations highly depends on the modeling of the Reynolds-stress tensor as a measure for the statistical influence of turbulence on the mean flow.

The most commonly used turbulence models in an industrial environment are so-called eddy-viscosity models (e.g. [1, 2]), which link the Reynolds stresses to the shear rate of the mean flow via an eddy viscosity as a proportionality factor. Mostly one or two transport equations are solved to provide the eddy viscosity. Second-moment closure (SMC) models, on the other hand, directly employ transport equations for the Reynolds stresses, offering

a higher potential for an adequate predicition of complex flows. They are often refered to as Reynolds-stress models (RSM).

Recently Cécora et al. [3] presented a SMC model (JHh-v2) which showed promising results in different aeronautical applications, containing high-lift airfoil flow and shock/boundary-layer interaction. It was however noticed that the JHh-v2 model underestimates the development of turbulence in shear layers with inflection point in the velocity profile. Corresponding examples are the backward-facing step (BFS) flow, in which the slowly developing turbulence causes too long separation length, as well as the round turbulent jet, which exhibits an overestimated jet core length. A remedy is found by implementing an additional sink term, which is sensitized towards shear flows with inflection point, into the length-scale equation. The successful application of this term to a similar Reynolds-stress model (RSM-P_{SAS}) has already been shown by Maduta [4] and Jakirlić and Maduta [5]. The two RSM are both evolved from the JH model [6], they mainly differ in the length-scale equation, with the JHh-v2 employing the homogeneous dissipation rate ε^h as length-scale variable while the RSM-P_{SAS} model uses the homogeneous part of the inverse time scale $\omega^h = \varepsilon^h/k$. Furthermore the JHh-v2 model contains an additional source term in the length-scale equation which sensitizes the model towards adverse pressure gradients. Last but not least the models use a different set of coefficients in the length-scale equation.

In this paper, the extension and calibration of the JHh-v2 model is presented, using a backward-facing step flow and a zero-pressure-gradient flat plate flow as calibration cases. The resulting model is named as JHh-v3. The performance of the JHh-v3 model is validated considering two wall-bounded transonic flows as well as a turbulent round jet.

2 NUMERICAL METHOD

The following investigations have been carried out using the DLR-TAU Code [7], a finite-volume solver which solves the Favre- and Reynolds-averaged Navier-Stokes equations on hybrid unstructured grids with second order accuracy.

Closure of the equation system is achieved with a differential Reynolds-stress turbulence model. It is based on a near-wall RSM by Jakirlić and Hanjalić [6] (JH RSM), which was implemented into the DLR-TAU Code by Probst and Radespiel [8]. A re-calibration for different aeronautical test cases was conducted by Cécora et al. [3], resulting in the model version JHh-v2, which is further developed in this work.

2.1 Extension of the JHh-v2 Model for Free Shear Flows

It was noted that the current version of the Reynolds-stress model (JHh-v2) tends to underestimate the growth of Reynolds stresses in free shear layers which contain an inflection point in the velocity distribution. As a remedy, an additional sink term is implemented into the length-scale equation with the intention of locally reducing dissipation and hence supporting the development of turbulence. After implementation, the RSM is

re-calibrated and named as JHh-v3.

The background of the implemented sink term can be found within the $k-kL$ model of Rotta [9], which employs a transport equation for the quantity kL, with L being an integral length scale of turbulence:

$$kL = \frac{3}{16} \int_{-\infty}^{\infty} R_{ii}\left(\vec{x}, r_y\right) dr_y \ . \tag{1}$$

R_{ij} describes the two-point correlation tensor of the velocity fluctuation u_i', considering the Einstein summation convention for R_{ii}. In the derivation of the modeled kL equation from an exact transport equation, Rotta notices a second production term that is influential on the performance of his turbulence model. Menter and Egorov [10] proposed their own way of modeling this term, furthermore they transformed it to different length-scale variables in order to make it suitable for modern turbulence models [10, 11]. This second production term contains second derivatives of the velocity tensor, which enables the turbulence model to account for additional length scales within the mean velocity field. Combining it with an eddy-viscosity model gave birth to the so-called Scale Adaptive Simulation (SAS) concept [10], in which the turbulence model is sensitized for resolving instabilities by locally reducing modeled turbulence. The additional source term especially contributes in shear flows with velocity distributions containing inflection points, which is an indicator for a tendency towards instability. Combined with the length-scale equation of modern eddy-viscosity models, the source term reduces the modeled turbulence in the affected region, causing the simulation to develop unsteadiness. Using these turbulence models with SAS-extension in a time-accurate flow solver (URANS) allows for an improved prediction of turbulence in shear layers with a tendency towards instability. Instead of combining the additional source term to an eddy-viscosity model, Maduta and Jakirlić [12] use the SAS concept in combination with a second-moment closure model.

While the SAS concept is intended to resolve a wide part of the turbulent spectrum in unsteady flow regions, the opposite approach followed in this work is to consider a wider spectrum of instabilities within the turbulence model. Therefore the SAS source term is used as a sink term in the length-scale equation of the Reynolds-stress model:

$$\frac{D\varepsilon^h_{(JHh-v3)}}{Dt} = \frac{D\varepsilon^h_{(JHh-v2)}}{Dt} - P_{SAS} \ . \tag{2}$$

This idea was proposed and successfully applied by Maduta [4] using the JH Reynolds-stress model in combination with a ω^h length-scale equation. After transformation of Maduta's term into an ε^h formulation, the implemented sink term reads:

$$P_{SAS} = C_{SAS,1} \max\left[P_{SAS,1} - P_{SAS,2}, 0\right] \ , \tag{3}$$

with

$$P_{SAS,1} = 1.755 \kappa k S^2 \left(\frac{L}{L_{vk}}\right)^{\frac{1}{2}} \tag{4}$$

and

$$P_{SAS,2} = 3k^2 \max\left(C_{SAS,2}\frac{(\nabla\varepsilon^h)^2k^2 + (\nabla k)^2(\varepsilon^h)^2 - 2k\varepsilon^h\nabla\varepsilon^h\nabla k}{k^2(\varepsilon^h)^2}, \frac{(\nabla k)^2}{k^2}\right) . \qquad (5)$$

The formulation contains the turbulent length scale $L = k^{3/2}/\varepsilon^h$ and the 3D generalization of the classical boundary-layer definition of the von Karman length scale $L_{vk} = \kappa S/\left|\nabla^2 U\right|$.

3 CALIBRATION OF THE ADDITIONAL SINK TERM

Although the model investigated in this work is derived from the same Reynolds-stress model as the one shown by Maduta [4] and as Maduta and Jakirlić [5], minor differences can be found in the formulations and in the model coefficients. Therefore the sink term can not be just transformed from ω^h to ε^h, it has to be calibrated as well. The additional sink term (Eq. (3)-(5)) contains two coefficients that need to be calibrated: $C_{SAS,1}$ and $C_{SAS,2}$, where the former is responsible for the global impact of the term compared to the regular source terms. The latter modifies the term itself.

In Fig. 1, the distribution of the ratio of $P_{SAS,1}$ and the main destruction term Y_{ε^h}[1] is shown for the backward-facing step flow, simulated with the basic JHh-v2 RSM. A strong contribution can be seen in the developing shear layer between the recirculating flow and the outer flow. Furthermore significant values are found in the boundary layer upstream of the step, very close to the wall.

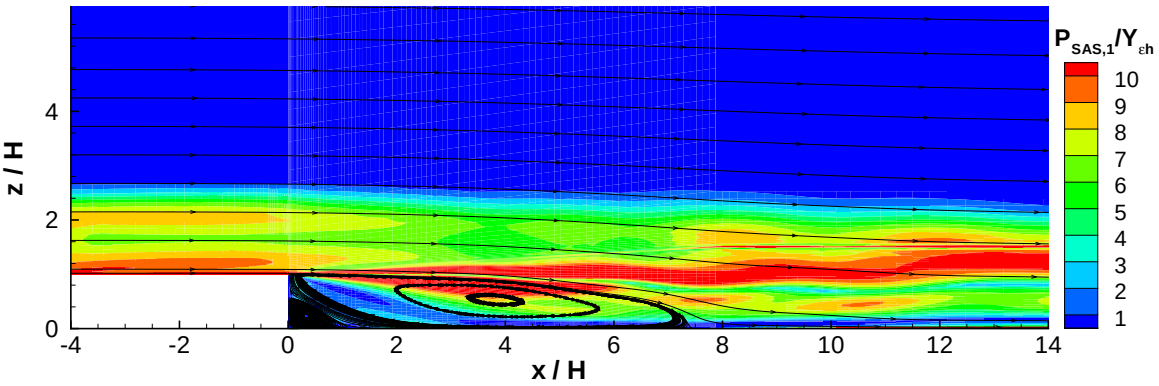

Figure 1: BFS. Ratio of $P_{SAS,1}$ to main destruction term Y_{ε^h}.

Corresponding profiles of $P_{SAS,1}$ at two different streamwise positions, upstream of the

[1]Due to the modeling formulation of a combined production-destruction, i.e. derived from two terms in the exact ε equation, the sink term is originally refered to as $P_\varepsilon^4 - Y$ [13]. As a simplification and in order to illustrate its function as destruction term of the ε^h equation, the sink term is in this work denoted as Y_{ε^h}.

step ($x/H = -4$) as well as near the center of the recirculation region ($x/H = 4$), can be seen in Fig. 2.

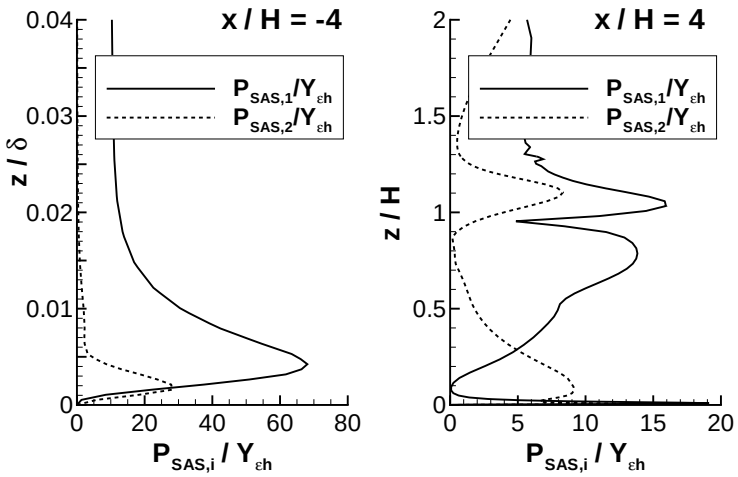

Figure 2: BFS. Ratio of $P_{SAS,1}$ and $P_{SAS,2}$ to main destruction term Y_{ε^h}; $C_{SAS,1} = 0.008$, $C_{SAS,2} = 2.0$

The second part $P_{SAS,2}$ has its main contribution very close to the wall, as well as in the upper part of the shear layer. As an outcome of Eq. 3 for the sink term, the distribution of $P_{SAS,2}$ is subtracted of the distribution of $P_{SAS,1}$.

As one can see from the skin-friction coefficient in Fig. 3, the basic JHh-v2 model predicts a recirculation zone which is considerably too long. Introducing the first part of the P_{SAS} term with a negative sign into the length-scale equation amplifies the turbulence production within the developing shear layer, leading to a shortened recirculation zone. Due to the increased turbulence in the near-wall boundary layer, the skin-friction is higher upstream of the step as well as in the recovering boundary layer downstream of the recirculation zone. The intensity of both effects, earlier reattachment and higher skin friction in the boundary layer, can be adjusted by the coefficient $C_{SAS,1}$.

Considering the second contribution to P_{SAS}, the near-wall peak of $P_{SAS,2}$ in Fig. 2 (left) reduces the boundary-layer skin friction, while the reattachment point is only slightly influenced (Fig. 3). With increasing $C_{SAS,2}$, the skin friction is further reduced, simultaneously the influence on the recirculation zone rises. Therefore c_f can not be corrected by modifying $C_{SAS,2}$ only. Within the original model, the low-Reynolds production term $P_{\varepsilon 3}$ with the coefficient $C_{\varepsilon 3} = 0.7$ can be used for this purpose. By increasing the coefficient $C_{\varepsilon 3}$, the skin friction can be reduced.

In Fig. 4, the turbulent shear stress distribution in a profile immediately downstream of the step at $x/H = 1$ can be seen. While the basic RSM drastically underestimates the turbulence in the shear layer, $P_{SAS,1}$ can help to improve the prediction. The amplifying effect of $P_{SAS,1}$ is reduced by increased coefficients for $P_{SAS,2}$ and $P_{\varepsilon 3}$.

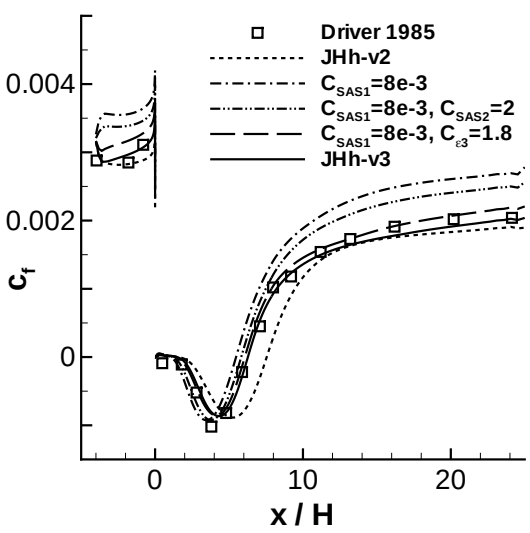

Figure 3: BFS. Skin-friction coefficient along the wall.

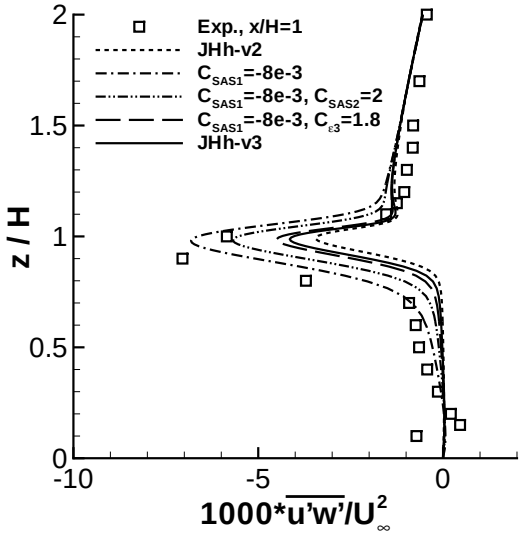

Figure 4: BFS. Profile of turbulent shear stress at streamwise position $x/H = 1$.

For a precise adjustment of the skin friction in boundary layers, a zero-pressure-gradient (ZPG) flat plate has to be simulated. As we have already seen in the backward-facing step flow, the skin friction rises when $P_{SAS,1}$ is activated (Fig. 5).

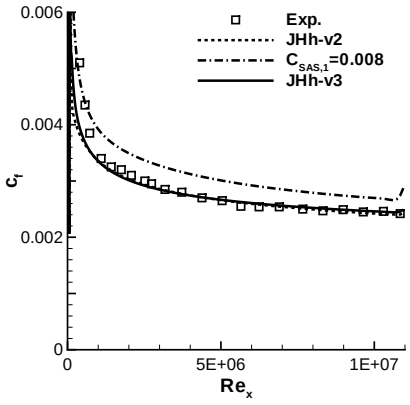

Figure 5: Zero-Pressure-Gradient Flat Plate. Skin-friction coefficient along the wall.

Agreeable results for both calibration cases, backward-facing step as well as ZPG flat plate, are achieved for the following coefficient set: $C_{SAS,1} = 0.008$, $C_{SAS,2} = 2.0$, $C_{\varepsilon 3} = 1.8$. The resulting model is named as JHh-v3. When the shear-stress profile in Fig. 4 is considered, even higher values of $C_{SAS,1}$ seem appropriate to obtain agreeable turbulence

levels. The coefficients found here are however regarded as a reasonable compromise of the cases investigated so far.

4 VALIDATION OF THE EXTENDED MODEL

Since the model formulation and its coefficients are changed, the new turbulence model version has to be validated against different test cases, in order to evaluate its performance for a wide range of aeronautical flows.

4.1 Round Single-Stream Jet

Similar to the backward-facing step flow, a shear layer with inflection point develops between a jet and the stagnant or slowly moving ambiance. The turbulent M = 0.75 jet that emerges from a round nozzle was simulated on a hexahedral mesh with $9 \cdot 10^6$ points. Velocity profiles as well as profiles of the turbulent shear stress component $\overline{u'v'}$ can be seen in Fig. 6, in comparison to experimental results [14].

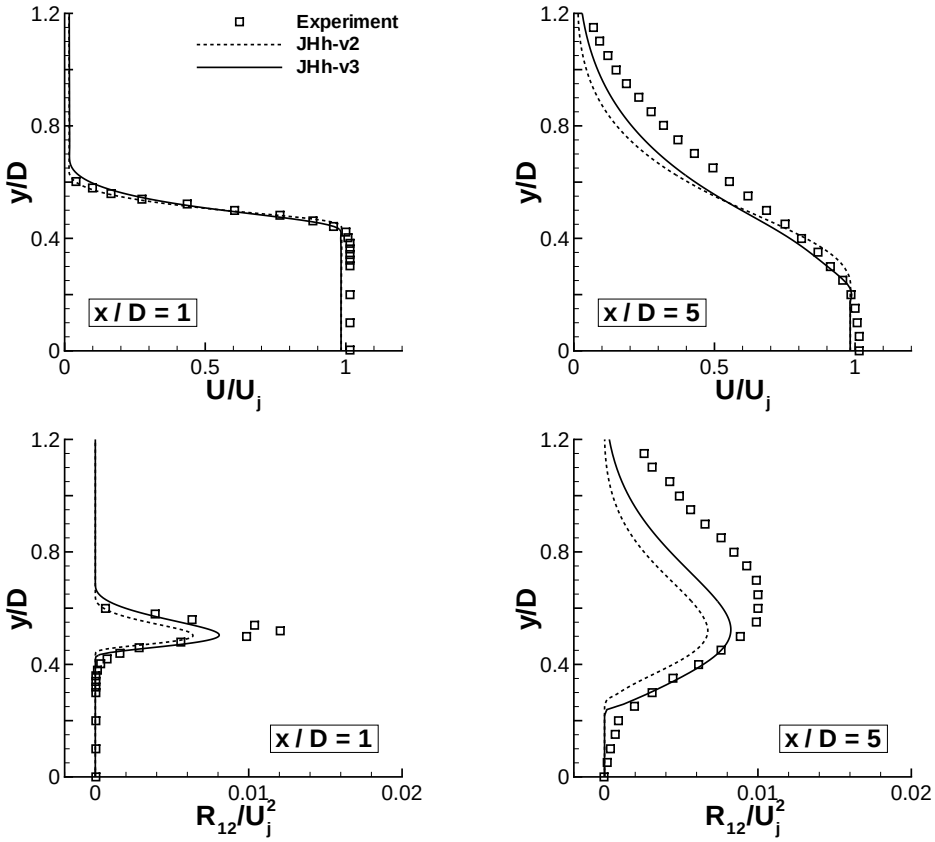

Figure 6: Round Single-Stream Jet. Profiles of velocity (upper line) and turbulent shear stress (lower line), at two streamwise positions.

Already early in the developing shear layer ($x/D = 1$, with x having its origin at the nozzle exit), the JHh-v2 model underestimates the turbulent shear stress, similarly to the BFS flow. The lack of turbulence is still existent at $x/D = 5$, showing furthermore an influence on the velocity profile. An improvement is found in the simulation with the JHh-v3 model, where higher levels of turbulence increase the transport of momentum, giving a velocity profile with a better agreement to the experimental data. Nevertheless the peak values of $\overline{u'v'}$ are underpredicted.

The underestimated transport of momentum has a lengthening effect on the jet core, which can be seen in Fig. 7. The velocity on the jet axis is shown for both RSM versions

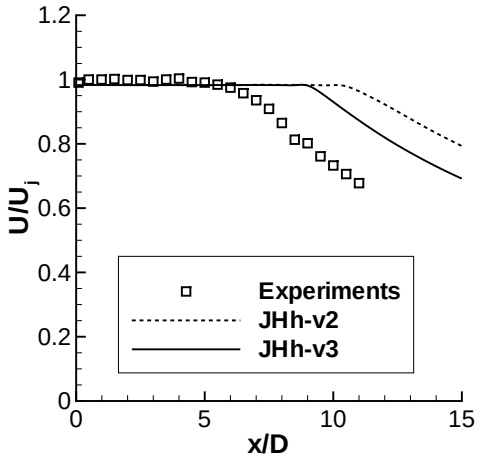

Figure 7: Round Single-Stream Jet. Axial velocity ratio along the jet axis.

as well as for the experiments, with U_j being the axial velocity at $x/D = 0$. While in experiments the axial velocity starts to decrease at $x_c/D = 5...6$, JHh-v3 predicts $x_c/D \approx 8.8$ and JHh-v2 even $x_c/D \approx 10.4$.

4.2 Transonic Airfoil RAE 2822

The supercritical flow around the RAE 2822 airfoil is a standard test case for turbulence models, experimental data is provided by Cook et al. [15]. Fig. 8 shows a comparison of measured and simulated pressure distribution at Mach number M = 0.73 and Reynolds number Re = $6.5 \cdot 10^6$, also known as Case 9. It can be seen that the influence of the additional sink term in combination with the re-calibration is rather small for this fully attached airfoil flow. A small contribution can be found in the decelerated boundary layer near the shock, increasing the turbulence and therefore stabilizing the boundary layer. As a result, the shock moves slightly downstream.

4.3 Transonic Axisymmetric Bump

The flow at transonic Mach number over an axisymmetric bump is a complex test case for turbulence models. It develops a compression shock which interacts with the boundary layer and induces a flow separation over the rear part of the bump, before it reattaches further downstream. Experiments have been conducted by Bachalo and Johnson [16, 17]. The axisymmetric problem was simulated on a 2D grid of 48000 points that was rotated by 5°, employing an axisymmetry boundary condition on both sides. The 2D grid contains 300 points in streamwise direction, of which 150 discretize the bump geometry. The boundary layer upstream of the bump is resolved by 90 points in wall-normal direction.

In order to adequately predict the shock location as well as the separation point, a good quality of the turbulence model in simulating the upstream boundary layer through favorable and adverse pressure gradient is essential. The reattachment point however strongly depends on the turbulent shear stresses that develop in the separated shear layer.

Fig. 9 shows a comparison of the simulated pressure distribution with experiments. It can be noticed that the basic JHh-v2 model overestimates the size of the separation,

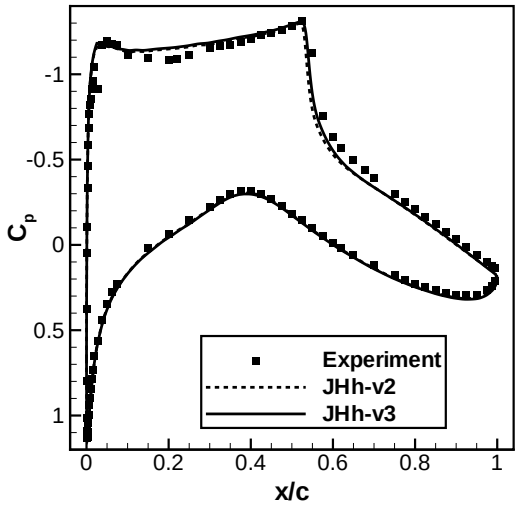

Figure 8: Transonic Airfoil RAE 2822, Case 9. pressure coefficient along the airfoil.

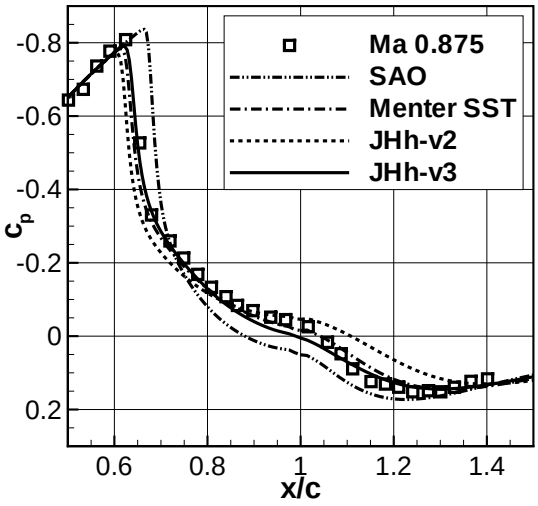

Figure 9: Transonic Axisymmetric Bump. Pressure coefficient along the wall.

which results in an exaggerated pressure plateau around $x/c = 1$. Furthermore the shock position is found slightly upstream of the experimental prediction. Clear improvements of the pressure distribution can be found when using the JHh-v3 model, especially in the recovering boundary layer downstream of the separation ($x/c \approx 1.2$). The pressure plateau is even underestimated, while the shock position shows a good agreement to the

experimental data. A comparison of shock position, separation location and reattachment location is given in Tab. 1.

Table 1: Transonic Axisymmetric Bump. Comparison of simulated and measured flow topology.

	SAO	Menter SST	JHh-v2	JHh-v3	Exp.
Shock position[2]	0.690	0.645	0.633	0.653	0.66
Separation point	0.690	0.645	0.667	0.689	0.70
Reattachment point	1.165	1.174	1.194	1.092	1.10
Length of separation	0.475	0.529	0.527	0.403	0.40
Distance of separation to shock	0.000	0.000	0.034	0.036	0.04

It can be noticed that the prediction of the reattachment point and thus the length of the separation is improved in the simulation with JHh-v3. Furthermore the shock moves slightly downstream, similar to the RAE 2822 case. While both eddy-viscosity models show an immediate separation at the shock, the boundary layer endures the adverse pressure gradient for a short distance in the simulations with both RSM versions, which agrees to the experimental data.

5 CONCLUSION

The extension of the length-scale equation of a differential Reynolds-stress turbulence model with an additional sink term has been presented. It was shown that the modification amplifies the development of turbulence in free shear flows, which positively influences the separation length of a backward-facing step flow. Furthermore the overprediction of the core length in turbulent round jets is reduced. Only minor influence is noticed in the simulation of the attached flow around the transonic airfoil RAE 2822, whereas the prediction of the separated flow over a transonic bump is improved.

Acknowledgments

The authors gratefully acknowledge the "Bundesministerium für Bildung und Forschung" who funded parts of this research within the frame of the joint project *AeroStruct* (funding number 20 A 11 02 E), as well as the "North-German Supercomputing Alliance" for supplying us with computational resources within the project *niii00090*. Furthermore we would like to thank A. Probst of DLR Göttingen who provided a computational mesh and his experience for the BFS flow.

[2]In the simulations, the shock position is not a discrete point. The measured shock position corresponds to a pressure coefficient of $c_p = -0.49$, which was used for determination of the simulated shock positions.

REFERENCES

[1] Spalart, P. R., Allmaras, S. R. A one-equation turbulence model for aerodynamic flows. *La Recherche Aèrospatiale* (1994) **1**:5–21.

[2] Menter, F. R. Two-Equation Eddy-Viscosity Turbulence Models for Engineering Applications. *AIAA Journal* (1994) **32(8)**:1598–1605.

[3] Cécora, R.-D., Eisfeld, B., Probst, A., Crippa, S. and Radespiel, R. Differential Reynolds Stress Modeling for Aeronautics. *50th AIAA Aerospace Sciences Meeting* (2012) Nashville, Jan. 9-12.

[4] Maduta, R. An eddy-resolving Reynolds stress model for unsteady flow computations: development and application. *Dissertation*, TU Darmstadt (2014).

[5] Jakirlić, S. and Maduta, R. On "Steady" RANS Modeling for improved Prediction of Wall-bounded Separation. *52nd AIAA Aerospace Sciences Meeting* (2014) National Harbor, MD, USA.

[6] Jakirlić, S. and Hanjalić, K. A new approach to modelling near-wall turbulence energy and stress dissipation. *Journal of Fluid Mechanics* (2002) **459**:139–166.

[7] Schwamborn, D., Gardner, A., von Geyr, H., Krumbein, A., Lüdeke, H. and Stürmer, A. Development of the TAU- Code for aerospace applications. *50th NAL International Conference on Aerospace Science and Technology* (2008) Bangalore, India.

[8] Probst, A. and Radespiel, R. Implementation and Extension of a Near-Wall Reynolds-Stress Model for Application to Aerodynamic Flows on Unstructured Meshes. *46th AIAA Aerospace Sciences Meeting and Exhibit* (2008).

[9] Rotta, J. C. *Turbulente Strömungen.* Stuttgart: B. G. Teubner (1972).

[10] Menter, F. R., and Egorov, Y. A Scale-Adaptive Simulation Model using Two-Equation Models. *AIAA-Paper 2005-1095* (2005).

[11] Menter, F. R., and Egorov, Y. The Scale-Adaptive Simulation Method for Unsteady Turbulent Flow Predictions. Part 1: Theory and Model Description. *Flow, Turbulence and Combustion* (2010) **85(1)**:113-138.

[12] Maduta, R., and Jakirlić, S. An eddy-resolving Reynolds stress transport model for unsteady flow computations. In: Advances in Hybrid RANS-LES Modelling 4. *Notes on Numerical Fluid Mechanics and Multidisciplinary Design.* (2012) **117**: 77-89.

[13] Jakirlić, S. A DNS-Based Scrutiny of RANS Approaches and Their Potential for Predicting Turbulent Flows. *Habilitationsschrift*, TU Darmstadt (2004).

[14] Jordan, P., Gervais, Y., Valière, J.-C. and Foulon, H. Final results from single point measurements. *Project deliverable D3.4, JEAN - EU 5th Framework Programme, G4RD-CT2000-00313* (2002) Laboratoire dEtude Aérodynamiques, Poitiers.

[15] Cook, P. H., McDonald, M. A., Firmin, M. C. P. Aerofoil RAE 2822 – Pressure Distributions, and Boundary Layer and Wake Measurements. In: J. Barche (Ed.), *Experimental Data Base for Computer Program Assessment* (1979) AGARD-AR-138 **A6**.

[16] Bachalo, W. D., and Johnson, D. A. An Investigation of Transonic Turbulent Boundary Layer Separation Generated on an Axisymmetric Flow Model. *AIAA 12th Fluid and Plasma Dynamics Conference* (1979) Williamsburg, Virginia.

[17] Bachalo, W. D., and Johnson, D. A. Transonic, Turbulent Boundary-Layer Separation Generated on an Axisymmetric Flow Model. *AIAA Journal* (1986) **24(3)**:437-443.